Biomaterials 33 (2012) 731–739

Contents lists available at SciVerse ScienceDirect

Biomaterials

journal homepage: www.elsevier.com/locate/biomaterials

Cell adhesion, spreading, and proliferation on surface functionalized with RGD nanopillar arrays

Md. Abdul Kafi [a,1], Waleed Ahmed El-Said [a,1], Tae-Hyung Kim [b], Jeong-Woo Choi [a,b,*]

[a] Interdisciplinary Program of Integrated Biotechnology, Sogang University, 35 Baekbeom-Ro, Mapo-Gu, Seoul 121-742, Republic of Korea
[b] Department of Chemical & Biomolecular Engineering, Sogang University, 35 Baekbeom-Ro, Mapo-Gu, Seoul 121-742, Republic of Korea

ARTICLE INFO

Article history:
Received 11 August 2011
Accepted 1 October 2011
Available online 20 October 2011

Keywords:
Three-dimensional peptide nanostructures
Cell-substrate interaction
RGD peptide
Cell functions
Cofilin phosphorylation

ABSTRACT

In this paper, a method was introduced for the fabrication of vertically and spatially-controlled peptide nanostructures that enhance cell adhesion, proliferation, spreading on artificial surfaces. The RGD nanostructures with different heights were fabricated on gold surfaces by self-assembly technique through a nanoporous alumina mask composed of nanoscale-controlled pores. Pore diameter and spatial distribution were controlled by manipulating the pore widening time at a constant voltage during the mask fabrication process. Two-dimensional RGD nanodot, three-dimensional RGD nanorod, and RGD nanopillar arrays were carried out using various concentrations of RGD peptide solution, self-assembly times, and pore sizes, which were 74 nm, 63 nm, and 43 nm in diameter, respectively. The fabricated RGD nanodot, nanorod, and nanopillar arrays were utilized as a cell adhesion layer to evaluate the cell adhesion force, adhesion speed, spreading assay, and phosphorylation of cofilin protein in PC12, HeLa, and HEK293T normal cells. Among the three different nanostructures, RGD nanopillar arrays were found to be suitable for cellular attachment, spreading, and proliferation due to the proper arrangement of the RGD motif, which mimics *in vivo* conditions. Hence, our newly fabricated RGD nanostructured array can be successfully applied as a bio-platform for improving cellular functions and in *in vitro* tissue engineering.

1. Introduction

Cell-based research or biotechnology has been intensively applied in a variety of fields, such as pharmacology, medicine, cell biology, toxicology, basic neuroscience, and environmental monitoring. The diverse application of cell-based techniques is due to the useful information that can be obtained from living cells, a basic building block of all kinds of living organisms. Using cells, the effects of drugs, toxins, or functional particles can be easily monitored, which is not possible in protein/DNA analysis or in animal-based tests. Consequently, cell-artificial surface interactions have attracted considerable attention due to the difficulty of cell immobilization on artificial surfaces while maintaining *in vivo*-like conditions, which is the most important factor in *in vitro* research. Several previous studies reported the adhesion efficiency of cells on various kinds of materials such as cover glass, ITO-coated glass, and bare gold surfaces [1,2]. A variety of biological molecules including carbohydrates, cell-extracellular matrix (ECM) proteins or their components (e.g., Arginine-glycine-aspartic acid (RGD), and poly-L-lysine (PLL)) have been introduced to reduce the variation in cell attachment and to increase the cell binding affinity to the bottom surface, which is essential for providing *in vivo*-like conditions [3–6]. Since biological cell systems are normally regulated by the arrangement of extracellular proteins and their interactions at the molecular level, more research related on cells and artificial ECM are needed in order to determine the structural characteristics of ECM proteins, their assemblies in nano-scale, and their uncovered effects on target cells.

Therefore, modification of bio-ligands on artificial surfaces is very promising for fabrication of the next generation of nanobio-platforms [7–9]. A variety of research has focused on the control of protein/peptide assembly techniques for fabrication of topologically-altered structures at micrometer scale or sub-micrometer scale [9–16]. These ligand-modified surfaces were previously found to be effective for various kinds of cellular functions such as cell adhesion; mineralization, and gene expression [17–20]. However, alteration of an artificial surface for fabrication

* Corresponding author. Department of Chemical and Biomolecular Engineering, Sogang University, Seoul, Republic of Korea. Tel.: +82 2 705 8480; fax: +82 2 3273 0331.
E-mail address: jwchoi@sogang.ac.kr (J.-W. Choi).
[1] Md. Abdul Kafi and Waleed A. El-Said contributed equally to this work.

0142-9612/$ – see front matter © 2011 Elsevier Ltd. All rights reserved.
doi:10.1016/j.biomaterials.2011.10.003

of a cell friendly environment mostly requires methods that are proper for the modification of 2D spaces. Since cells naturally exist in 3D environments, many ECM proteins also exist as 3D structures, which is more suitable for attachment to the cell membrane and for connection to the cell. Hence, the performances of synthetic peptide or ECM components that are frequently used to enhance cell attachment can be improved by 3D nanopatterning technology, which establishes real *in vivo*-like conditions. Previous research reported the fabrication of a 3D-nanopatterned substrate based on common nanopatterning techniques that utilize physical or electrochemical deposition of metal or functional polymers [21]. The fabricated 3D nanostructures were found to be proper for cell adhesion; however, the surfaces of the 3D nanostructures still need to be modified with ECM protein or its components for effective cell adhesion, which is laborious and time-consuming. Moreover, ECM proteins cannot be modified equally to the whole surfaces of 3D nanostructures and may cause structural variations in the fabricated surface.

We previously reported several RGD peptides that include a terminal cysteine residue for the efficient fabrication of a peptide mono-layered gold (Au) surface [4]. Since the sulfide group in cysteine can be attached onto a gold surface by a strong Au–S covalent bond [3,4] 2D-RGD peptide-modified surface could be simply obtained by self-assembly. Among the several cysteine-containing RGD peptides, RGD-MAP-C peptide containing quadruple branches of the repetitive RGD sequence was shown to be the best for cell adhesion and proliferation on artificial surfaces [3]. This RGD-MAP-C peptide was further integrated into the various kinds of cell chips and was found to increase the electrochemical signals from cells that largely contribute to the sensitive detection of the effects of anticancer drugs or environmental toxins [3,4]. Recently, we also found that 2D dot-like formation of RGD-MAP-C peptide significantly enhances the adhesion strength of neural cells between the cell membrane and electrode surface compared to the RGD-MAP-C mono-layered surface [3]. Hence, we hypothesized that controlled 3D-RGD nanopatterned surface will further enhance the many cellular functions of various kinds of cell lines.

Herein, we report 3D peptide nanostructured arrays fabricated by nanoporous alumina mask-assisted self-assembly technique. RGD-MAP-C peptide was chosen as a suitable candidate for establishing strong link at cell–substrate interface which can mimic in vivo-like environment. Three-dimensional RGD-MAP-C nanostructures were established with different heights (nanorod and nanopillar) on Au surfaces and its corresponding cell functions including cell spreading, attachment and proliferations were confirmed by scanning electron microscopy (SEM), atomic force microscopy (AFM) and trypan blue exclusion assay. Western blotting assay was further conducted to measure protein expression of the cells attached to the different substrates due to the fact that cofilin phosphorylation increased with increasing stretch ability of the actin skeleton via interaction between the RGD sequence and its integrin during cellular spreading [22–28]. Finally, MTT assay was performed to compare the mitochondrial activities of neuronal (PC12) and non-neuronal (HEK293T) cells attached to different kinds of peptide-modified surfaces, all of which utilized RGD-MAP-C peptide for surface functionalization.

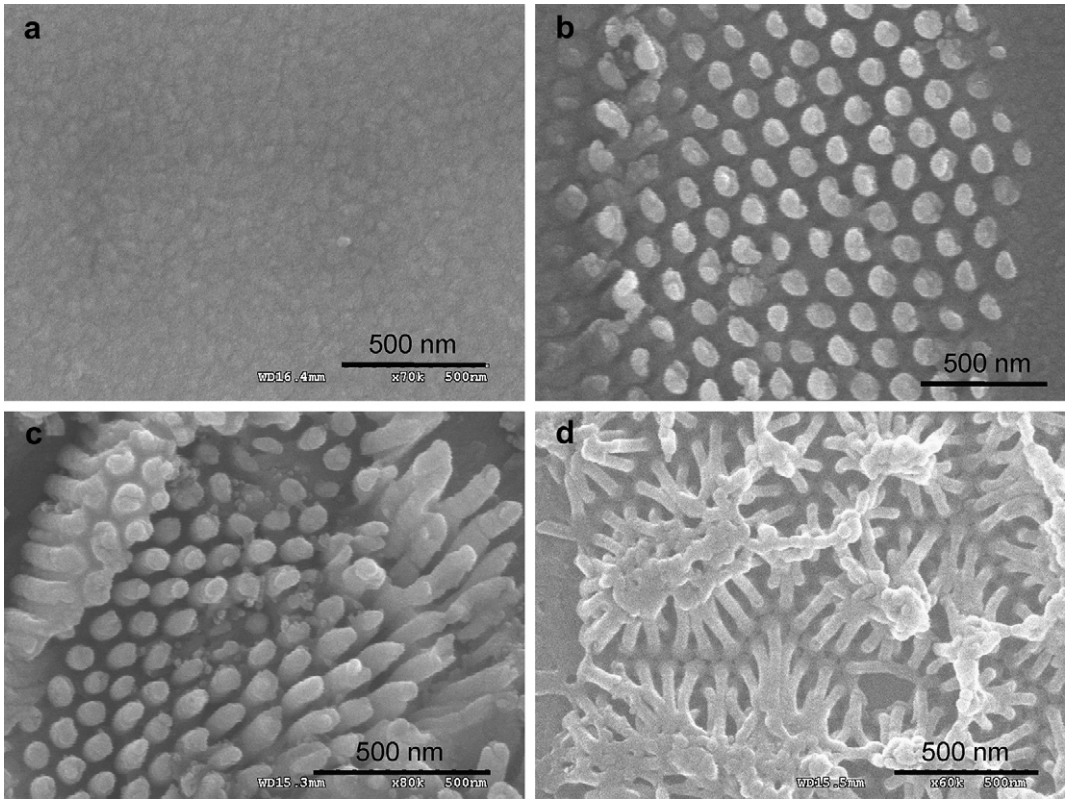

Fig. 1. Representative scanning electron microscopic (SEM) images of the Au surfaces employed in the cell experiments. The images obtained at 20 Hz from the sample pre-coated with Pt–Pd alloy. (a) Freshly cleaned bare Au surface prior to peptide immobilization, (b) 2D-RGD nanodot, (c) 3D-RGD nanorod, and (d) 3D-RGD nanopillar arrays. Scale bar 500 nm. Scanning electron microscopy (SEM) images were obtained using a field emission scanning electron microscope (Hitachi-S-4300) operating at an acceleration voltage of 20 kV and current 15 μA. All samples were coated with a conductive 3–5 nm sputtered platinum–palladium alloy layer prior to analysis. Working distance and magnification for (a) 16.4 mm and 70k times; (b) 15.3 mm and 70k times; (c) 15.3 mm and 80k times; and (d) 15.5 mm and 60k times, respectively.

2. Materials and methods

2.1. Materials

All solvent and reagents were of *puriss* grade quality and were used as received. Our designed cysteine (Cys)-modified RGD oligopeptide (RGD-MAP-C) was synthesized by Peptron (Daejeon, 305-340, South Korea). The peptides were dissolved in phosphate buffered saline (PBS; pH 7.4, 10 mM), which was purchased from Sigma–Aldrich (St. Louis, MO, USA).

2.2. Nanoporous alumina template synthesis

The nanoporous alumina template used in this work was prepared using a typical two-step anodization process on aluminum foil (99.99%, 100 mm in thickness) [29]. Briefly, the surface of the aluminum foil was electro-polished at 20 V in a mixed solution of perchloric acid and ethanol (1:4 in volume) for 60 s. The first anodization was performed by applying a DC voltage of 40 V in 0.3 M oxalic acid solution at 3 °C for 8 h. In order to obtain a well-ordered nanoporous alumina layer, the alumina layer formed during the first anodization process was completely removed by chemical wet etching in a mixture solution of phosphoric acid (0.4 M) and chromic acid (0.2 M) at 65 °C for 4 h. After removal of the anodic oxide layer, a second anodization process was conducted on the Al substrate under identical conditions to those used for the first anodization (Supplemental Table S1). After the second anodization, the surface of the nanoporous alumina was painted with a coating layer consisting of a mixture of nitrocellulose and polyesterresin in butylacetate, ethylacetate, and isopropyl alcohol. For preparation of the through-hole alumina masks, the remaining aluminum substrate was removed in saturated $HgCl_2$ solution. Then, the alumina barrier layer at the bottom of the cylindrical nanochannel of the alumina layer was etched out in 5 wt% phosphoric acid at 30 °C. To obtain the alumina template with through-holes, the coating layer was dissolved in acetone. The porous alumina was investigated using an atomic force microscope (Nanoscope digital instrument) at a scan rate of 1.00 Hz with a phosphorous (*n*) doped silicon cantilever. The size of the pore was determined by section analysis.

2.3. RGD nanostructures fabrication

Peptide nanostructured array was prepared through the nanoporous AAO template as described [3]. For all biological activity experiments, nanostructured peptide arrays were prepared on silicon-based gold and pretreated with piranha solution (H_2SO_4:H_2O_2, 7:3 v/v) [30,31], then extensively rinsed with de-ionized water and dried under N_2. The nanoporous AAO template was then fixed on the freshly cleaned Au surface. Subsequently, modified RGD peptide terminated with a Cysteine amino acid was deposited on the substrates by incubating 0.01–0.1 mg/ml of the peptide in PBS solution on the substrates for 12–24 h at 4 °C (Supplemental Table S1). After deposition, the AAO template was rinsed with DIW. In this way, the Cys-modified RGD was immobilized covalently on gold substrate directly without any organic linker materials [3]. The fabricated nanostructured surface was investigated using a field emission scanning electron microscope (Hitachi-S-4300) at an accelerated voltage of 2 kV from Pt/Pd alloy-coated samples, and freshly cleaned Au substrate served as a control.

2.4. Cell culture

Rat pheochromocytoma (PC12), human cervical (HeLa), and human embryonic kidney (HEK293) cells were purchased from Korean cell line bank. RPMI 1640 Medium (RPMI 1640, purchased from Fresh media®, Daegu, 704-230, South Korea) was used for PC12 while Dulbecco's modified Eagle's medium (DMEM, Gibco, Invitrogen, Grand Island, USA) supplemented with 10% heat inactivated fetal bovine serum (FBS; Gibco, Carlsbad, CA, USA), and 1% concentration of antibiotics (Gibco) was used for HeLa and HEK293 cells. Cells were maintained under standard cell culture conditions at 37 °C in an atmosphere of 5% CO_2. The medium was changed every 2 days. When the cells reached sub-confluence, they were harvested with trypsin and sub-cultured. The cells from three to six passages were used in the experiments.

2.5. Cell adhesion speed and adhesion strength on nanostructured RGD-modified Au surface

Cell adhesion speed was determined by trypan blue exclusion assay. The cell–substratum adhesion strength was measured by using centrifugation adhesion assay to obtain the fraction of adherent cells after centrifugation at a defined force as a metric of comparison. For the cell adhesion assay, nanostructured RGD-modified Au surfaces (10 mm × 10 mm size) were placed in a 24-well culture plates, and cells were seeded at a density of 5×10^4 cells/ml overnight under standard cell culture conditions.

2.6. SEM and AFM images of cellular morphology on nanostructured platform

Cell spreading assay was performed by analyzing the images obtained from SEM and leaser scanning confocal microscopy. For SEM imaging, PC12 cells were seeded

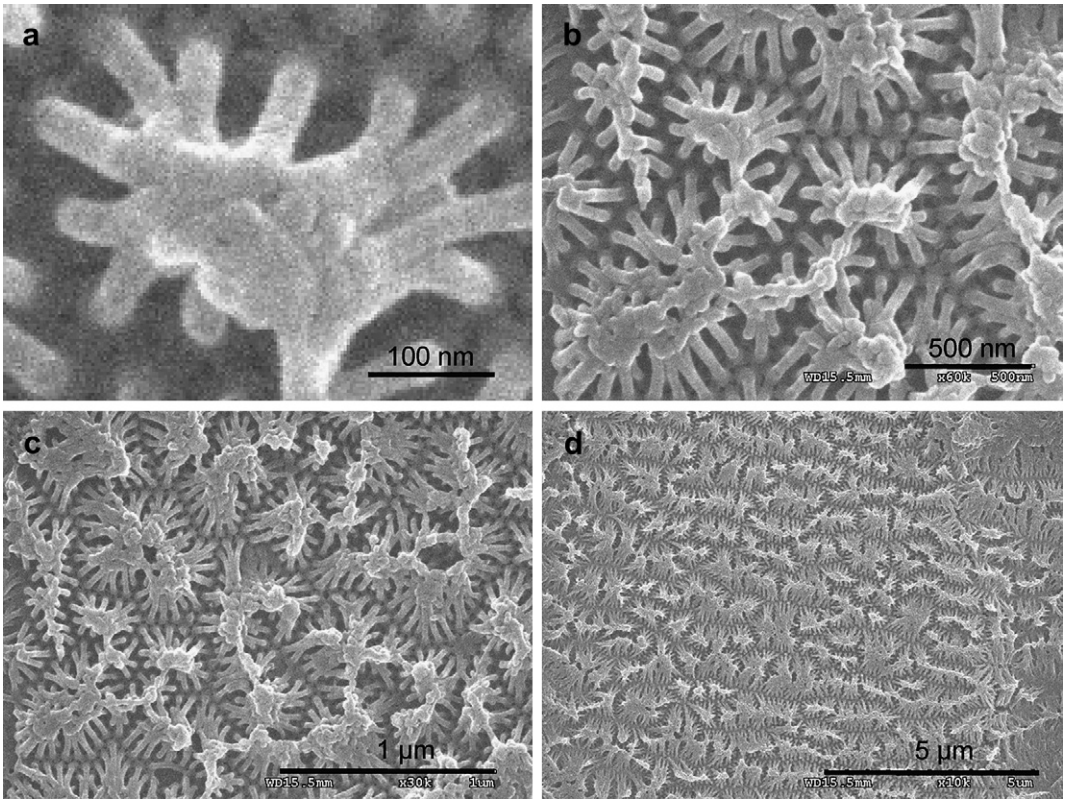

Fig. 2. Reproducibility of peptide nanoarray synthesis; images obtained from several areas of the fabricated surface at 100 nm (a), 500 nm (b), 1 μm (c), and 5 μm (d) scale bar.

on the peptide-modified Au surface. After incubation for 6 h at 37 °C, cells were washed twice with PBS, fixed in 4% paraformaldehyde in phosphate buffer, and coated with Pt/Pb alloy before imaging. The images were obtained using a field emission scanning electron microscope (Hitachi-S-4300) at an accelerated voltage of 2 kV from Pt/Pd alloy-coated samples. Furthermore, the morphologies of the living cells immobilized on the different RGD nanostructure-modified Au substrates were investigated for to determine cell spreading by AFM (NT-MDT, Russia) in semi-contact mode at room temperature with an inverted optical microscope. The maximum scan-range of the system was 100 μm in the both *x* and *y* axes. The cantilevers were NSG01 type, which had a typical resonant frequency in the range of 115–190 kHz and a force constant of 2.5–10 N/m. The scan rate was 1 Hz.

2.7. MTT assay

Tetrazolium dye (MTT) was used to assess cellular function. MTT assay is a non-toxic, soluble, colorimetric redox indicator that changes color in response to cell metabolism. In this study, 5×10^4 cells were seeded on the top of the peptide-coated Au surface (10 mm × 10 mm size) placed in 24-well plates. After 2 days of culture, cells were incubated in MTT (0.5 mg/ml)/culture media in a humidified atmosphere at 37 °C and 5% CO_2 for 4 h. Then, media was excavated and 200 μl of dimethylsulfoxide (DMSO) was added to dissolve precipitated formazan. Finally, 100 μl of solution was transferred to 96-well plates and measured at 590 and 630 nm in order to determine the percentage of MTT reduction.

2.8. Western blot analysis

To determine the level of cofilin phosphorylation, cells were lysed with lysis buffer (50 mM Tris–HCl, pH 6.5, 10% glycerol, 2% SDS, 2% 2-mercaptoethanol) at 95 °C for 5 min and sonicated. After centrifugation, supernatants were collected and the protein concentration determined using BCA protein assay reagent (Pierce Chemicals). For Western blot analysis, cell lysates proteins were separated on SDS-PAGE and transferred onto polyvinylidene difluoride membranes (Bio-Rad, Hercules, CA). The membrane was blocked with 4% nonfat dry milk in PBS containing 0.05% Tween 20 for 1 h at room temperature and incubated overnight with anti-cofilin antibody (abcam, Cambridge Science park, Cambridge, UK), anti-P-cofilin antibody (abcam, Cambridge Science park, Cambridge, UK), and anti-actin antibody diluted in PBS containing 1% nonfat dry milk and 0.05% Tween 20. After washing in PBS containing 0.05% Tween 20, the membrane was incubated with horseradish peroxidase-conjugated anti-mouse IgG (Amersham Pharmacia Biotech). Immunoreactive protein bands were visualized by exposing the membrane for 10 s to 2 min to ECL chemiluminescence reagent (Amersham Pharmacia Biotech).

2.9. Statistical analysis

All values are expressed as mean ± standard deviation, and all experiments were repeated at least three times. Data were analyzed using the computerized statistical program 'Origin 8'. Significant differences were determined for $p < 0.05$.

3. Results and discussion

3.1. Fabrication of peptide nanostructured array

For *in vitro* cell analysis, efficient attachment of cells onto artificial surfaces with minimum ECM materials requires convenient patterning. Nanoimprinting and photolithographic technique are well-established for the patterning of biomaterials using PDMS coupled with photolithography or laser etching technique [32–35]. Our group recently developed mask-guided, spatially-controlled nanopatterned ECM [3]. In this work, we introduced a method for the fabrication of a vertically-controlled 2D/3D-nanostructured RGD array on silicon-based Au surfaces using a controlled nanoporous AAO mask. Well-ordered nanoporous alumina layers were prepared using the two-step anodization process described by Masuda [29]. The pore diameters and spatial distributions were controlled by adjusting the pore widening period at a constant voltage as shown in Supplemental Table S1. Supplemental Fig. S1 shows AFM images of the three different nanoporous AAO masks with diameters of 74, 63, and 43 nm that were used for future studies. These nanopore diameters showed significant effects on the deposition of peptide and allowed for convenient patterning on Au support. Therefore, using these three different masks, spatially and vertically-controlled 2D-RGD nanodots, 3D-RGD nanorods, and 3D-RGD nanopillars array were achieved when different concentrations of RGD peptide (0.01 mg/ml–0.1 mg/ml) were deposited at 4 °C for 12 h, 18 h, and 24 h, respectively, as shown in Supplemental Fig. S2 and Supplemental Table S1.

Fig. 1b shows that uniform 2D-RGD nanodots formed periodic patterns with an average distance of separation of 35 nm. The average diameter of the nanodots formed on the Au substrate was 70–75 nm. Clearly, accurate positioning of the RGD ligand molecules formed a replica of the mask, despite the problems inherent in their growth under homogeneous distribution. The 2D-RGD dots with controlled size and uniformity in their spatial distribution were achieved reproducibly by using nanoporous AAO masks. The close-packed hexagonal pore array of the AAO played a very important role in determining the ordering of the nanostructures. Therefore, changes in the pore diameter and pore density of the nanoporous AAO masks allowed the diameter and density of the nanodot array to be modified. Fig. 1c demonstrated that the 3D-RGD nanorod array with a diameter of 60 nm and a spatial distance of 45 nm was obtained when 0.1 mg/ml of RGD was immobilized through the mask with pores 62 nm in diameter. Interestingly, vertical growth of the peptide nanostructure was observed here. We found that well-ordered rods formed due to the reduction of pore diameter and increase in deposition time [36,37]. Therefore,

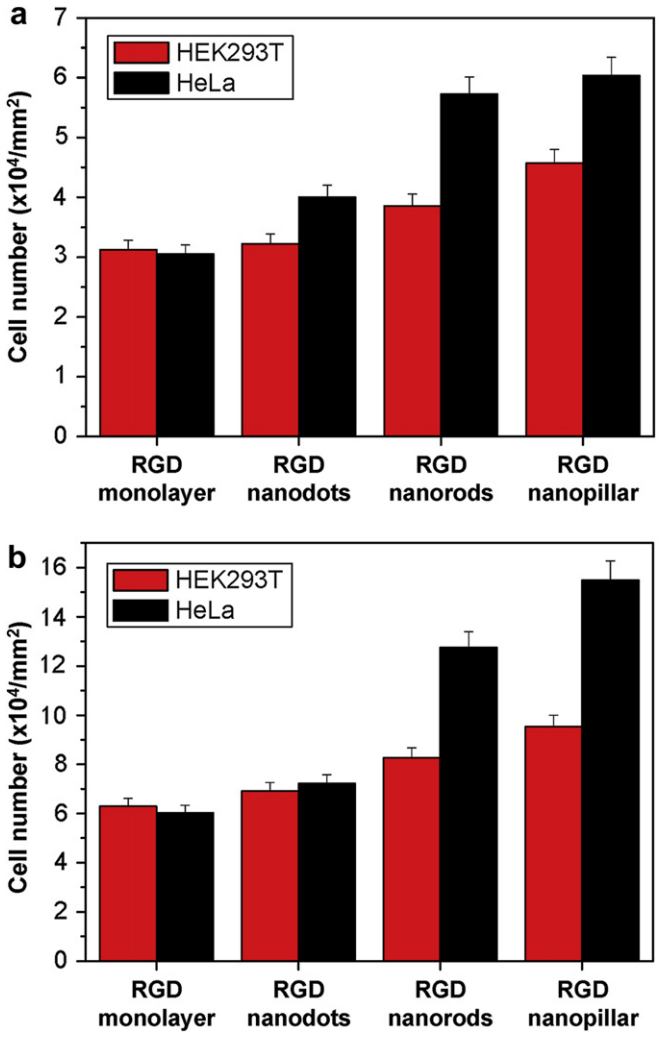

Fig. 3. (a) Evaluation of adhesion cell speed of HEK293T and HeLa cells on various nanostructured RGD-modified Au surfaces after 1 h of cell culture using trypan blue dye assay. (b) Cell adhesion strength of HEK293T and HeLa cells on various nanostructured RGD-modified Au surfaces after 1 day of cell culture using trypan blue dye assay. Data are the mean ± standard deviation of three different experiments.

we repeated the experiment using more precisely controlled pores (43 nm). More vertical growth was observed, resulting in a pillar-like structure with a featured diameter of 35–40 nm and a spatial distance of about 65–70 nm (Fig. 1d). Fig. 2a shows the 3D-RGD nanopillar array, where 10–12 pillar heads coalesced to form an integrin receptor site at a distance of around 125–150 nm. Reproducibility of the 3D-RGD nanopillar arrays is shown in Fig. 2b–d. A large area of the nanopillar array is shown with different scale bars, 500 nm (Fig. 2b), 1 μm (Fig. 2c), 5 μm (Fig. 2d), and zoomed image of a single scaffold (Fig. 2a) for cellular integrin receptor [38]. These results confirm that self-assembly of RGD peptide through nanoporous AAO mask has potential for the fabrication of 3D-RGD peptide nanostructures with a control diameter and morphology that can be covalently bonded to Au substrate at accurate positions.

3.2. *Effect of fabricated RGD nanostructures on cell adhesion speed and attachment strength*

The cell adhesion speed and parallel cell attachment strength assays were performed to assess the variations among the fabricated RGD nanostructures. For this, cell adhesion speed of HeLa (cancer) and HEK293T (normal) cells on 2D-RGD nanodots, 3D-RGD nanorods, and 3D-RGD nanopillar-coated Au substrates were compared with the RGD monolayer-coated Au substrate based on trypan blue dye assay [38]. Cell adhesion speed experiments were carried out by seeding the cells on RGD monolayer/Au, RGD nanodots/Au, RGD nanorods/Au, and RGD nanopillars/Au for 1 h, after which non-bound cells were washed off by PBS. Then, cell densities on the different substrates were detected as shown in Fig. 3a. RGD nanodot/nanorod/nanopillar-functionalized Au substrates induced cell adhesion, resulting in high cell densities. In contrast, low cell density was observed for RGD the monolayer-modified surface, which demonstrates that the cells remained only loosely attached to the RGD monolayer-modified Au surface.

Cell adhesion strength based on the characteristics of RGD ligand arrangement reportedly affects cell adhesion speed [39]. The cell-substratum adhesion strength was detected by using centrifugation adhesion assay to obtain the fraction of adherent cells after centrifugation at a defined force as a metric of comparison [39,40]. Cell adhesion strength assay was performed for normal and cancer cells immobilized on the nanostructure RGD arrays. Fig. 3b shows the densities of cells adhered to the nanopatterned RGD-modified Au surfaces in comparison with non-patterned RGD monolayer-modified Au. The results show that the cell adhesion strength was higher on the 3D-RGD nanopillar-modified Au substrate. This trend was also observed in the presence of the 2D-RGD nanodot and 3D-RGD nanorod-modified Au substrates. However, cells adhered to non-patterned RGD monolayer-modified Au substrates showed low cell/substratum adhesion strength. Therefore, the enhancement of cell adhesion strength could have positive effects

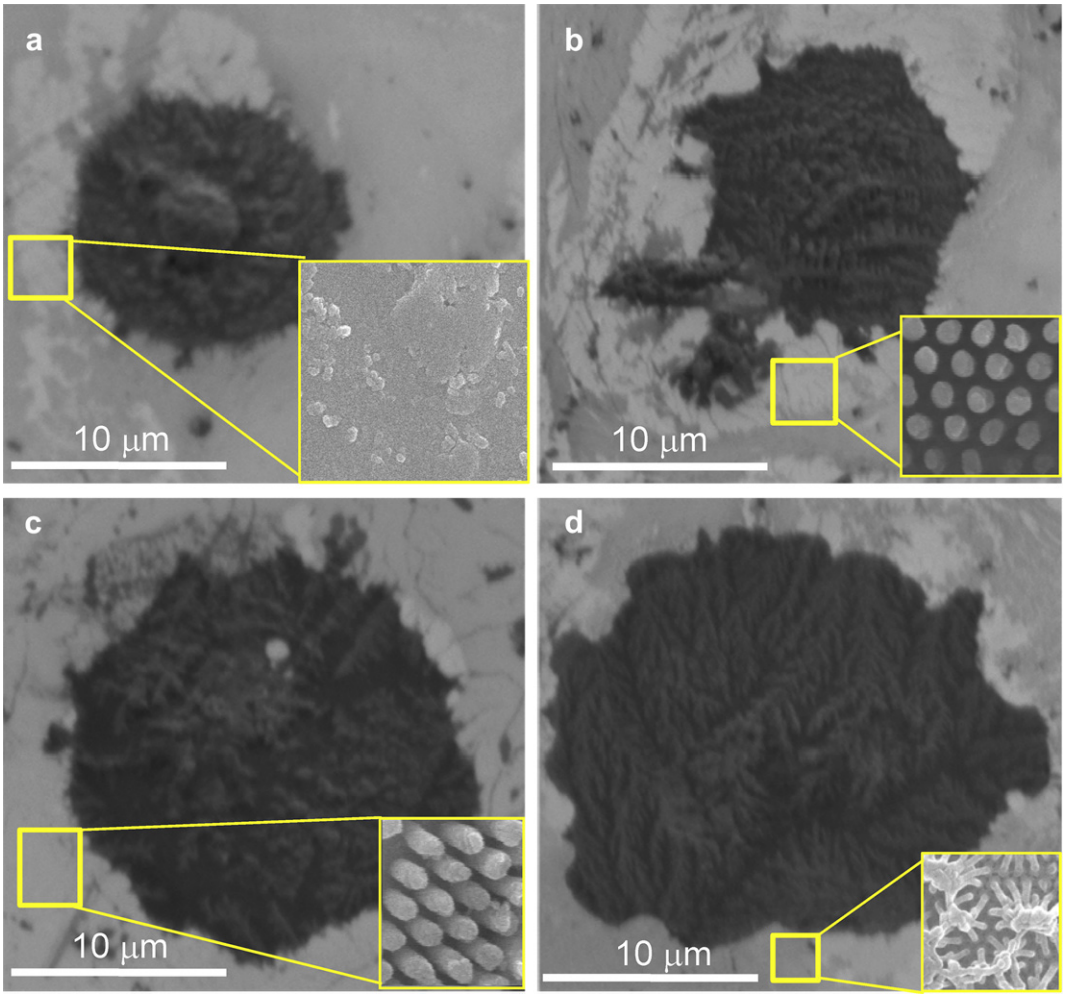

Fig. 4. Scanning electron microscopic (SEM) images obtained from formalin-fixed cells after 6 h of cell culture on non-patterned RGD monolayer (a), and nanopatterned 2D-RGD nanodot (b), 3D-RGD nanorod (c), and 3D-RGD nanopillar arrays (d). The insets show corresponding zoomed images of the fabricated surfaces. Scale bar 10 μm.

on cellular behavior, including cell spreading, integrin clustering, and cytoskeletal interactions, compared to non-uniformly distributed focal complexes [10–16,38].

3.3. Effect of fabricated RGD nanostructures on cell spreading

Three selected topographic RGD peptide-modified Au surfaces were evaluated to identify the suitable patterned array for cell attachment and spreading. Imaging techniques such as scanning electron microscopy (SEM) and leaser scanning confocal microscopy were used to monitor the spreading of PC12 cells on RGD non-patterned monolayer and patterned 2D-RGD nanodots, 3D-RGD nanorods, and 3D-RGD nanopillars. Fig. 4 shows the SEM images for PC12 cells that were spread over the nanostructured pattern for 6 h after seeding. Highest spreading was noticed on the 3D-RGD nanopillar array (Fig. 4d), moderate spreading on the 3D-RGD nanorod (Fig. 4c) and 2D-RGD nanodot array (Fig. 4b), and lowest spreading on the non-patterned RGD monolayer (Fig. 4a). This significant variation in spreading was due to the variation in tractions forces [18] of the 2D-RGD nanodots, 3D-RGD nanorods, and 3D-RGD nanopillars during cytoskeletal growth [22]. Moreover, the uniformity and spatial distribution of the highly ordered 3D-RGD nanopillar array (Fig. 2) properly matched that of integrin receptor on the cell membrane, which favors cellular attachment and spreading [18–20].

Cellular spreading was further investigated by analyzing the morphological images obtained from live cells using AFM. Fig. 5a shows that the cells on non-patterned RGD monolayer displayed a round morphology with limited fillapodial spreading. In contrast, the cells on the 2D- or 3D-nanopatterned RGD-modified Au substrates showed well-spread morphology and exhibited an elongated shape in the opposite direction as the cytoplasmic extensions. These extensions were predicted to function in communication between cells or in anchoring the cells to the peaks of the surfaces (Fig. 5b–d). The highest spreading was observed in the 3D-RGD nanopillars array compared to the other topographic RGD nanopattern (Fig. 5d). The extension of plasma membrane in all directions combined with a distinctly increased surface area was the highest in cells on 3D-RGD nanopillar-coated Au surfaces rather than cells on other topographical nanostructured substrates. Focal adhesions were established on all three RGD-modified Au substrates [38]. However, subtle differences in the size and type of the focal adhesions were observed depending on the pattern and morphology of the RGD peptide. Therefore, the cells on non-patterned RGD monolayer-modified Au surfaces were concluded to have lower motility than those on the topographic nanopatterned RGD-modified Au surface [35].

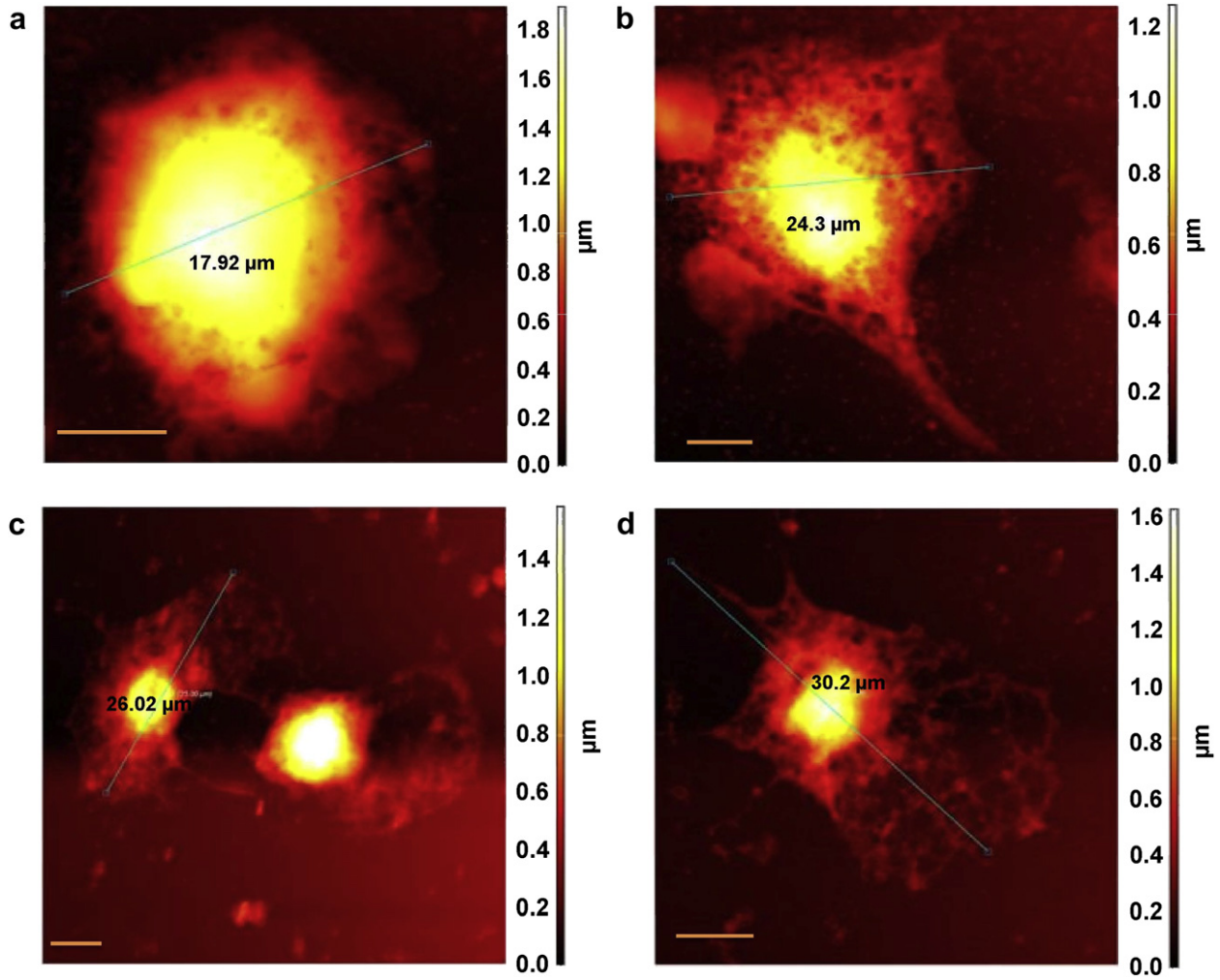

Fig. 5. Atomic force microscopic (AFM) images obtained from live cells after 24 h of cell culture on non-patterned RGD monolayer (a), 2D-RGD nanodot (b), 3D-RGD nanorod (c), and 3D-RGD nanopillar arrays (d). Scale bar 5 µm.

3.4. Effect of fabricated RGD nanostructures on cofilin phosphorylation

We next examined the effects of nanostructured peptide array on the phosphorylation activity of cofilin. PC12 cells and HEK293T cells cultured on various topographic nanopatterned RGD arrays were lysed and subjected to Western blot analysis using anti-cofilin and anti-p-cofilin as primary antibodies and anti-mouse IgG as secondary antibody. As shown in Fig. 6a and b, highest cofilin expression was observed in cells grown on RGD monolayer, lowest in cells on 3D-nanopillar arrays, and moderate in cells on 2D-RGD nanodot and 3D-RGD nanorod arrays. Interestingly, opposite findings were observed for p-cofilin expression, in which the highest p-cofilin expression was observed in cells grown on 3D-RGD nanopillar arrays and lowest in those on RGD monolayer. This variation in expression was due to the increased phosphorylation of cofilin in cells grown on topographic RGD-modified surfaces [28]. Fig. 6c and d showed that intensity of cofilin decreases with topographically altered RGD nanostructures which results the corresponding increase in p-cofilin level. Therefore, the highest p-cofilin expression and corresponding lowest cofilin expression in cells grown on 3D-RGD nanopillar array indicate maximum phosphorylation. Previously, it was reported that cofilin phosphorylation is related to cellular spreading and cytoskeletal stretch [26]. Cytoskeletal stretch depends on the attachment of the cellular receptor to the ECM or it components [26–28]. Therefore, the highest phosphorylation as well as wide spreading of the cells on the 3D-RGD nanopillar array proves the strongest RGD-integrin interaction compared to the other RGD nanostructures.

3.5. Cell function by MTT reduction assay

In MTT assay, the absorbance of MTT (3[4,5-dimethylthiazol-2-yl]-2,5-diphenyltetrazolium bromide) is proportional to the number of viable cells [41]. The ability of cells to proliferate and form a confluent layer on the different topographic nanopatterned RGD-modified Au surfaces in comparison with the non-patterned RGD-modified Au surfaces was studied. The result shows the evaluation of cell proliferation of HEK293T (Fig. 7a) and HeLa cells (Fig. 7b), which were seeded and incubated on RGD-modified Au surfaces for 4 days followed by MTT assay. Among the topographic patterns, 3D-nanostructured RGD nanopillar-modified Au substrates showed higher cell proliferation rates because their RGD motif orientation properly matched receptor-mediated binding with integrin receptors on the cell membrane [26–28]. Moreover, the proliferation rates of HEK293T and HeLa cells on the RGD nanorod array-modified Au substrate was significantly increased compared to that on RGD nanodot array-modified Au substrate, most likely due to the 3D structures of the RGD nanorods and pillars, which may have interacted with the integrin receptors on the cell surface membrane more easily. The experiment was repeated with PC12 cells and the results compared to HEK293T cells to confirm if there is any difference between the neural and normal cells. Fig. 8 demonstrates that for both cell types, the proliferation

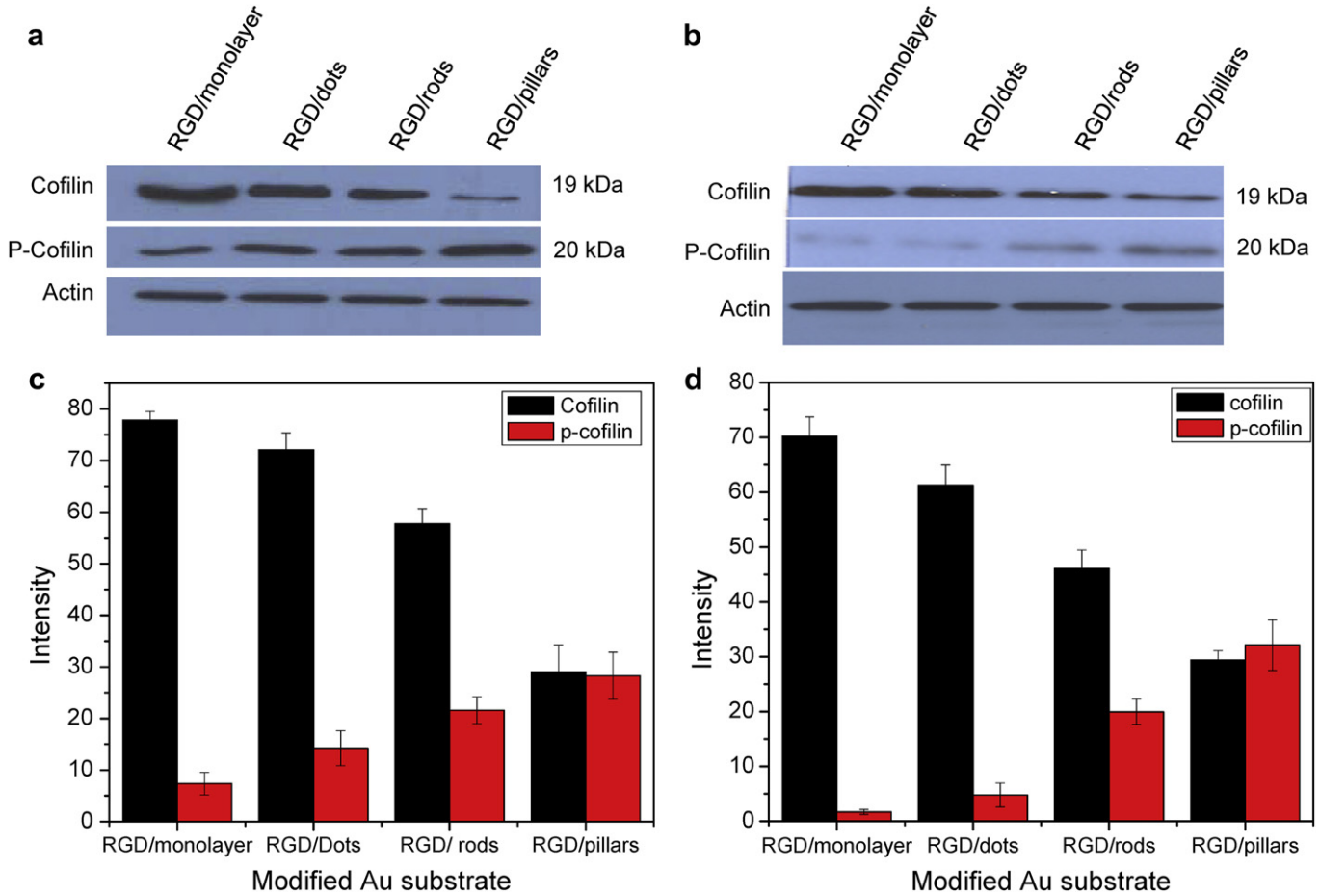

Fig. 6. Cofilin phosphorylation based on western blot assay: cofilin and p-cofilin levels in PC12 cells (a), HEK293T (b) cells seeded on different nanostructured RGD-modified Au surfaces. Intensity of cofilin and p-cofilin expression in PC12 (c) and HEK293T (d) cells obtained from three independent experiments performed at identical conditions.

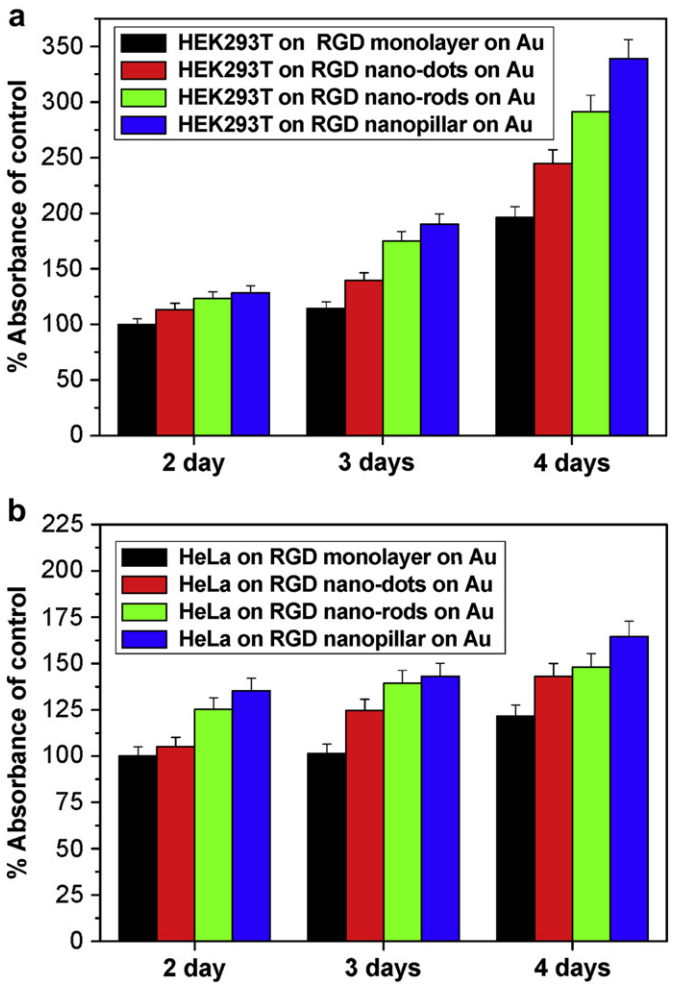

Fig. 7. Evaluation of cell proliferation of HEK293T cells (a) and HeLa cells (b) on different nanostructured arrays using MTT assay as percentage function of control absorbance for 4 days. Data are the mean ± standard deviation of six different experiments.

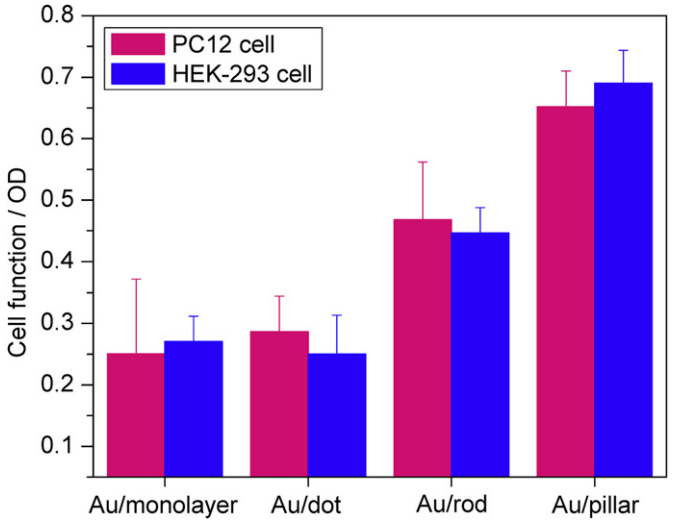

Fig. 8. Evaluation of cell function based on MTT reduction in PC12 cells and HEK293T cells seeded on various nanostructured RGD-modified Au surfaces as percentage function of control absorbance. Data are the mean ± standard deviation of six different experiments.

rate was significantly higher for the 3D-RGD nanostructured array compared to the other topographic structure, whereas no significance difference was observed between the cell lines. These results clearly show that the 3D-RGD nanostructured array properly represents the adhesion ligands for cellular receptors, resulting in strong cell-substrate interactions irrespective of the cell line.

4. Conclusions

In this study, we reported a simple bottom-up method for the fabrication of a RGD nanopillar array fully composed of RGD peptide based on simple self-assembly technique. The performance of the fabricated 3D nanostructure was intensively evaluated with respect to the cell adhesion speed, attachment strength, spreading, cofilin phosphorylation, and mitochondrial activity. Cell functions significantly increased on the 3D-RGD-MAP-C nanopatterned surface compared to the RGD-MAP-C monolayer and 2D nanodot surface, regardless of the cell line. Among the 3D peptide nanostructures, 3D-nanopillar array was more suitable for cell adhesion and spreading than the 3D nanorod array due to the increased binding sites for integrin receptor on the cell surface that contribute to the formation of a strong link between the cells and Au. This superiority of 3D-nanopillar array is very important since the maintenance of *in vitro* cell culture conditions that mimic the *in vivo* environment is a challenging task that must be overcome for effective drug screening and tissue engineering. Hence, our fabricated 3D-RGD nanopillar array-modified bio-platform can be applied for *in vitro* cell function assays as well as for the generation of tissue implants in regenerative medicine.

Acknowledgments

This work was supported by a National Research Foundation of Korea (NRF) grant funded by the Korea government (MEST) (2011-0000384), by the Nano/Bio Science & Technology Program (M10536090001-05N3609-00110) of the Ministry of Education, Science, and Technology (MEST), and by the Graduate School of Specialization for Biotechnology Program of the Ministry of Knowledge Economy (MKE).

Appendix. Supplementary data

Supplementary data associated with this article can be found, in the online version, at doi:10.1016/j.biomaterials.2011.10.003.

References

[1] Jin LH, Yang BY, Zhang L, Lin PL, Cui C, Tang J. Patterning of HeLa cells on a microfabricated au-coated ITO substrate. Langmuir 2009;25:5380–3.
[2] Choi CK, Margraves CH, Jun SI, English AE, Rack PD, Kihm KD. Opto-electric cellular biosensor using optically transparent indium tin oxide (ITO) electrodes. Sensors 2008;8:3257–70.
[3] Kafi MA, Kim T-H, Yea C-H, Kim H, Choi J- W. Effects of nanopatterned RGD peptide layer on electrochemical detection of neural cell chip. Biosens Bioelectron 2010;26:1359–65.
[4] Kafi MA, Kim T-H, An JH, Choi J- W. Electrochemical cell-based chip for the detection of toxic effects of bisphenol-A on neuroblastoma cells. Biosens Bioelectron 2011;26:3371–5.
[5] May KM, Wang Y, Bachas LG, Anderson KW. Development of a whole-cell-based biosensor for detecting histamine as a model toxin. Anal Chem 2004; 76:4156–61.
[6] Yea CH, Min J, Choi J-W. The fabrication of cell chips for use as bio-sensors. Biochip J 2007;1:219–27.
[7] Hutmacher DW. Scaffolds in tissue engineering bone and cartilage. Biomaterials 2000;21:2529–43.
[8] Dembo M, Wang Y-L. Stresses at the cell-to-substrate interface during locomotion of fibroblasts. Biophys J 1999;76:2307–16.
[9] Malmstroum J, Christensen B, Jakobsen HP, Lovmand J, Foldbjerg R, Sorensen ES, et al. Large area protein patterning reveals nanoscale control of focal adhesion development. Nano Lett 2010;10:686–94.

[10] Arnold M, Cavalcanti-Adam EA, Glass R, Blummel J, Eck W, Kantlehner M, et al. Activation of integrin functions by nanopatterned adhesive interfaces. ChemPhysChem 2004;5:383–8.
[11] Cavalcanti-Adam EA, Micoulet A, Blummel J, Auernheimer J, Kessler H, Spatz JP. Lateral spacing of integrin ligands influences cell spreading and focal adhesion assembly. Eur J Cell Biol 2006;85:219–24.
[12] Huang JH, Grater SV, Corbellinl F, Rinck S, Bock E, Kemkemer R, et al. Impact of order and disorder in RGD nanopatterns on cell adhesion. Nano Lett 2009;9:1111–6.
[13] Arnold M, Schwieder M, Blummel J, Cavalcanti-Adam EA, Lopez-Garcia M, Kessler H, et al. Cell interactions with hierarchically structured nano-patterned adhesive surfaces. Soft Matter 2009;5:72–7.
[14] Wolfram T, Spatz JP, Burgess RW. Cell adhesion to agrin presented as a nanopatterned substrate is consistent with an interaction with the extra-cellular matrix and not transmembrane adhesion molecules. BMC Cell Biol 2008;9:64.
[15] Lee T, Min J, Kim S-U, Choi J-W. Multifunctional 4-bit biomemory chip consisting of recombinant azurin variants. Biomaterials 2011;32:3815–21.
[16] Arnold M, Hirschfeld-Warneken VC, Lohmuller T, Heil P, Blummel J, Cavalcanti-Adam EA, et al. Induction of cell polarization and migration by a gradient of nanoscale variations in adhesive ligand spacing. Nano Lett 2008; 8:2063–9.
[17] Xia N, Thodeti CK, Hunt TP, Xu Q, Ho M, Whitesides GM, et al. Directional control of cell motility through focal adhesion positioning and spatial control of Rac activation. FASEB J 2008;22:1649–59.
[18] Fu J, Wang Y-K, Yang MT, Desai RA, Yu X, Liu Z, et al. Mechanical regulation of cell function with geometrically modulated elastomeric substrates. Nat Methods 2010;7:733–6.
[19] Aubin JE. Advances in the osteoblast lineage. Biochem Cell Biol 1998;76: 899–910.
[20] Rosen ED, Spiegelman BM. Molecular regulation of adipogenesis. Annu Rev Cell Dev Biol 2000;16:145–71.
[21] Kang SH, Pokroy B, Mahadevan L, Aizenberg J. Control of shape and size of nanopillar assembly by adhesion-mediated elastocapillary interaction. ACS Nano 2010;4:6323–31.
[22] Cavalcanti-Adam EA, Volberg T, Micoulet A, Kessler H, Geiger B, Spatz JP. Cell spreading and focal adhesion dynamics are regulated by spacing of integrin ligands. Biophys J 2007;92:2964–74.
[23] Dubin-Thaler BJ, Giannone G, Dobereiner H-G, Sheetz MP. Nanometer analysis of cell spreading on matrix-coated surfaces reveals two distinct cell states and steps. Biophys J 2004;86:1794–806.
[24] Ruoslahti E. RGD and other recognition sequences for integrins. Annu Rev Cell Dev Biol 1996;12:697–715.
[25] Pierschbacher MD, Ruoslahti E. Cell attachment activity of fibronectin can be duplicated by small synthetic fragments of the molecule. Nature 1984;309:30–3.
[26] Kafi MA, Kim T-H, An JH, Choi J-W. Fabrication of cell chip for detection of cell cycle progression based on electrochemical method. Anal Chem 2011;83: 2104–11.
[27] Tsumura Y, Toshima J, Leeksma OC, Ohashi K, Mizuno K. Sprouty-4 negatively regulates cell spreading by inhibiting the kinase activity of testicular protein kinase. Biochem J 2005;387:627–37.
[28] Niwa R, Nagata-Ohashi K, Takeichi M, Mizuno K, Uemura T. Control of actin reorganization by slingshot, a family of phosphatases that dephosphorylate adf/cofilin. Cell 2002;108:233–46.
[29] Masuda H, Fukuda K. Ordered metal nanohole arrays made by a two-step replication of honeycomb structures of anodic alumina. Science 1995;268: 1466–8.
[30] Choi J- W. Cell-based biochip to analyze the effect of anticancer drug. Biotechnol Bioprocess Eng 2005;9:12–20.
[31] Choi J-W, Nam YS, Fujihira M. Nanoscale fabrication of biomolecular layer and its application to biodevices. Biotechnol Bioprocess Eng 2004;9:76–85.
[32] Kustandi TS, Loh WW, Gao H, Low HY. Wafer-scale near-perfect ordered porous alumina on substrates by step and flash imprint lithography. ACS Nano 2010;4:2561–8.
[33] Liu Y, Weiss DN, Li J. Rapid nanoimprinting and excellent piezoresponse of polymeric ferroelectric nanostructures. ACS Nano 2010;4:83–90.
[34] Ahn SH, Guo LJ. Large-area roll-to-roll and roll-to-plate nanoimprint lithography: a step toward high-throughput application of continuous nanoimprinting. ACS Nano 2009;3:2304–10.
[35] Yim EKF, Reano RM, Pang SW, Yee AF, Chen CS, Leong KW. Nanopattern-induced changes in morphology and motility of smooth muscle cells. Biomaterials 2005;26:5405–13.
[36] Shingubara S, Okino O, Sakaue H, Takahagi T. Ordered two-dimensional nanowire array formation using selforganized nanoholes of anodically oxidized aluminum. Jpn J Appl Phys 1997;36:7791.
[37] Schwartz GC, Platter V. An anodic process for forming planar interconnection metallization for multilevel LSI. J Electrochem Soc 1975;122:1508.
[38] Maheshwari G, Brown G, Lauffenburger DA, Wells A, Griffith LG. Cell adhesion and motility depend on nanoscale RGD clustering. J Cell Sci 2000;113: 1677–86.
[39] Reyes CD, Garcia AJ. A centrifugation cell adhesion assay for high-throughput screening of biomaterial surfaces. J Biomed Mater Res A 2003;67:328–33.
[40] John JJSt, Schroen DJ, Cheung HT. An adhesion assay using minimal shear force to remove nonadherent cells. J Immunol Methods 1994;170:159–66.
[41] Bergamini A, Perno CF, Capozzi M, Mannella E, Salanitro A, Calio R, et al. A tetrazolium-based colorimetric assay for quantification of HIV-1-induced cytopathogenicity in monocyte-macrophages exposed to macrophage-colony-stimulating factor. J Virol Methods 1992;40:275–86.